Published in final edited form as:

Mol Cancer Ther. 2022 April 01; 21(4): 546–554. doi:10.1158/1535-7163.MCT-21-0821.

A Prostate Specific Membrane Antigen-Targeted Near-Infrared Conjugate for Identifying Pulmonary Squamous Cell Carcinoma During Resection

Gregory T. Kennedy[1], **Feredun S. Azari**[1], **Elizabeth Bernstein**[1], **Bilal Nadeem**[1], **Ashley Chang**[1], **Alix Segil**[1], **Neil Sullivan**[1], **Isvita Marfatia**[1], **Azra Din**[1], **Charuhas Desphande**[2], **John C. Kucharczuk**[1], **Philip Low**[3], **Sunil Singhal**[1]

[1]Department of Surgery, University of Pennsylvania School of Medicine, Philadelphia, PA

[2]Department of Pathology, University of Pennsylvania School of Medicine, Philadelphia, PA

[3]Department of Chemistry, Purdue University, West Lafayette, IN

Abstract

Pulmonary squamous cell carcinoma is the second-most common lung cancer subtype and has a low 5-year survival rate at 17.6%. Complete resection with negative margins can be curative, but a high number of patients suffer early postoperative recurrence due to inadequate disease clearance at the index operation. Intraoperative molecular imaging (IMI) with tumor-targeted optical contrast agents is effective in improving resection completeness for other tumor types, but there are no IMI tracers targeted to pulmonary squamous cell carcinoma. In this report, we describe the use of a novel prostate specific membrane antigen (PSMA)-targeted near-infrared conjugate (OTL78) to identify pulmonary squamous cell carcinoma. We identified PSMA as a viable target by examining its expression in human lung tumor specimens from a surgical cohort. 94% of tumors expressed PSMA in either the pulmonary squamous cells or in the tumor neovasculature. Using *in vitro* and *in vivo* models, we found that OTL78 reliably localized pulmonary squamous cell carcinoma in a PSMA-dependent manner. Lastly, we found that IMI with OTL78 markedly improved surgeons' ability to identify residual disease after surgery in a preclinical model. Ultimately, this novel optical tracer may aid surgical resection of pulmonary squamous cell carcinoma and potentially improve long-term outcomes.

Introduction

Lung cancer continues to affect broad segments of the population, with over 130,000 deaths expected from pulmonary malignancies this year in the United States.[1] Complete surgical resection, as compared to chemotherapy or radiation alone, offers a nearly tenfold increase in the likelihood of cure for most lung cancers.[2] However, local and systemic recurrence affect 20% of patients undergoing curative-intent resection, due to incomplete disease clearance and positive margins at the index operation.[3] To aid in the completeness of cancer

Corresponding Author: Sunil Singhal, MD, Department of Surgery, University of Pennsylvania Perelman School of Medicine, 3400 Spruce Street, 6 White Building, Philadelphia, PA 19104.

Disclosures: Dr. Low is a shareholder in OnTarget Laboratories. All other authors have no disclosures.

resection—and thus improve patient survival—intraoperative molecular imaging (IMI) is an important new tool in surgical oncology. The technology uses fluorescent, tumor-targeted tracers that can be detected by wavelength-specific cameras to identify positive margins and preoperatively unrecognized sites of disease.[4]

Our group has extensively studied a folate receptor alpha (FRα) targeted tracer to identify folate receptor positive malignancies during resection.[5] This tracer (OTL38) has been shown to improve visualization of pulmonary adenocarcinomas, which express FRα at 10^5 fold higher than surrounding lung parenchyma.[6] A Phase 1 trial of IMI using this tracer in 20 patients demonstrated that IMI is safe and feasible in patients undergoing resection of pulmonary adenocarcinomas.[7] A subsequent multi-institutional Phase 2 trial of 110 patients showed that the FRα-targeted tracer was effective in improving operative outcomes for patients by detecting synchronous lesions not identified on preoperative imaging, localizing non-palpable, visually occult lesions, or identifying tumor-positive margins.[8]

Despite advances made in IMI for a number of different tumor types, there are no existing IMI tracers to target pulmonary squamous cell carcinoma which is the second-most common lung cancer subtype and has a particularly low 5 year survival rate at 17.6%.[9] To address this major unmet need, we sought to identify a molecular target for imaging pulmonary squamous cell carcinoma. Based on preliminary evidence in the literature, we identified prostate specific membrane antigen (PSMA) as a promising molecular target.[10,11]

PSMA is a membrane-bound binuclear zinc metallopeptidase with a short N-terminal cytoplasmic tail and a large extracellular domain. The bulk of the protein is oriented to the extracellular space where it binds and hydrolyzes a number of natural substrates.[12] The cytoplasmic tail interacts with several scaffold proteins which modulate PSMA endocytosis by caveolae-dependent and clathrin-coated pit-dependent mechanisms.[13,14] PSMA is internalized in a constitutive manner, but the internalization rate increases with binding of PSMA-specific molecules to the extracellular domain of the protein.[15] These findings are being exploited for the development of therapeutic approaches to target the delivery of toxins, drugs, and short-range isotopes to the interior of PSMA-expressing cells.[16,17] Upregulated PSMA expression has been found in many solid tumors, in both the neoplastic cells themselves as well as the tumor neovasculature endothelial cells (NECs).[18] Additionally, it is not expressed in normal lung or vascular endothelial cells, making it a highly specific target.[10]

In recent years, PSMA-targeted IMI tracers have shown promise in preclinical models of prostate cancer resection.[19] Several targeted, small-molecule based and antibody-based tracers have been developed and tested, showing highly specific prostate cancer labeling.[16,17,19-25] While their application beyond prostate cancer has been proposed, none have been tested in non-prostatic malignancies.[19]

In this study, we hypothesized that a PSMA-targeted NIR tracer (OTL78) could identify pulmonary squamous cell carcinoma in patients during lung cancer resection. First, we validated PSMA as a viable target by evaluating its expression in pulmonary tumors from a surgical population at our institution. We then evaluated the dosing, timing, and efficacy

of OTL78 *in vitro* and in murine models of pulmonary squamous cell carcinoma. Finally, we developed a xenograft model of positive resection margins and evaluated the ability of OTL78 to identify residual disease after resection.

Materials and Methods

Assessing PSMA Expression in Human Pulmonary Squamous Cell Carcinoma by Immunohistochemistry

Under a University of Pennsylvania Institutional Review Board-approved protocol, histologic specimens from 50 consecutive pulmonary squamous cell carcinoma resections were obtained from the Hospital University of Pennsylvania's Lung Biobank. Samples were prepared and immunostained for PSMA using anti-PSMA monoclonal antibody (107.1A4, Lifespan Bio, LS-C150527). Written informed consent was obtained from all patients and that the studies were conducted in accordance with the Declaration of Helsinki ethical guidelines.

Once stained, a certified pulmonary pathologist manually scored specimen using an established scoring system ranging from 0 to 3+ as previously described.[26] Briefly, a score of 0 corresponded with absence of staining, 1+ equaled faint staining on luminal borders, 2+ equaled moderate staining on apical and sometimes lateral borders, and 3+ indicated strong circumferential staining. The tumor was considered positive when more than 10% of malignant cells were positively stained. Overexpression of PSMA was defined as a score of 2+ or 3+. Using a multivariate model, several patient and clinicopathologic variables were analyzed to determine correlation with PSMA expression: patient age, gender, self-reported race (White, Black, or Other), smoking status (previous/current or never smoker), and tumor stage.

Study Drug and Spectroscopic Analysis

OTL78 (chemical formula: $C_{74}H_{86}N_7Na_7O_{27}S_4$, molecular weight: 1793.37 a.m.u.) is a high-affinity PSMA-targeting ligand coined DUPA linked to an NIR fluorophore named S0456. OTL78 (≥96% purity) was obtained via collaboration with Philip Low, PhD (Purdue University, West Lafayette, IN) and On Target Laboratories (West Lafayette, IN). OTL78 was synthesized and manufactured in compliance with Good Manufacturing Practices, and was stored at −20°C in vials containing 6 mg OTL78 free acid in 3 mL water. Before utilization, the frozen vials were thawed, vortexed, and then diluted with 0.9% NaCl, 5% dextrose or culture media.

To examine the optical properties of OTL78, we analyzed the compound diluted in various solvents using a UV visible/NIR spectrophotometer with a single monochromator and dual detector for the wavelength range from 190 to 2700nm (Jasco, Oklahoma City, OK). We found that OTL78 excites at a wavelength of 774–776 nm and has a peak emission of 794–796 nm.

Cell Lines

The human prostate cancer cell line 22rv1 was obtained from the American Type Culture Collection (Manassas, VA, USA) and was used as a positive control in our experiments given known high levels of PSMA expression. The human cervical cancer cell line KB was used as a negative control in experiments given negligible PSMA expression.[16] Two human lung squamous cell carcinoma cell lines, H1264 and H513, were obtained from the ATCC. The ATCC uses short tandem repeat profiling for testing and authentication of cell lines. Cells were thawed, subcultured, and expanded per ATCC recommendations, and stored in liquid nitrogen as cryopreserved aliquots within five passages of their purchase from ATCC.

Cell lines were maintained *in vitro* using media containing RPMI, 10% fetal bovine serum (FBS), 2 mmol/L glutamine, and 5 ug/mL penicillin/streptomycin. Cell lines were regularly tested and maintained negative for *Mycoplasma spp* using MycoAlert Mycoplasma Detection Kit (Lonza).

Evaluation of In Vitro Binding and Internalization of OTL78 in Human Pulmonary Squamous Carcinoma Cells by Fluorescence Microscopy

Cell lines were cultured on poly-L-lysine-coated glass coverslips in 6-well plates with RPMI media supplemented with 10% FBS, L-glutamine, and penicillin/streptomycin for 24 hours. For internalization time course studies, cells were treated with 200 nM LysoTracker (Invitrogen, Waltham, MA) for 2 hours prior to incubation with 20 nM OTL78. Coverslips were removed from culture after varying intervals (5 min, 10 min, 30 min, 60 min, 120 min, 180 min). To examine dose-dependence, cells were incubated with different concentrations of OTL78 (1 nM, 5 nM, 10 nM, 20 nM, 50 nM, 100 nM) for 2 hours. Following dye administration, coverslips were mounted on glass slides with ProLong Gold antifade reagent with DAPI (Fisher Scientific, Waltham, MA) and imaged on a Leica DM6 B fluorescence microscope (Leica Microsystems, Wetzlar, Germany).

OTL78 Pharmacokinetic and Biodistribution Studies

Under a protocol approved from the University of Pennsylvania IACUC, female, 6-8 week old, athymic nude mice bearing flank 22rv1 xenografts measuring 250 ± 50 mm^3 were randomized to intravenous OTL78 delivery at 3 dosage levels: 1.0 mg/kg, 2.0 mg/kg, and 4.0 mg/kg (n = 5 per dosing level). After tail vein injection, the fluorescence of tumor and background was recorded at several time points using the Pearl Trilogy *In Vivo* Imaging System (LI-COR Biosciences, Lincoln, NE). OTL78 fluorescence was obtained using the 800-nm channel, which utilizes an excitation light source of 785 nm and emission detection at 820 nm. Mean fluorescence of regions of interest (ROIs) were delineated over tumor sites and compared to surrounding soft tissue (background) to create a tumor-to-background ratio (TBR). After optimal dosing and timing was determined, mice bearing 22rv1 and KB flank tumors (n=3 per group) were administered 2 mg/kg OTL78 and sacrificed at 4 hours. Organs were harvested and imaged using the Pearl imaging system for biodistribution analysis.

Evaluation of In Vivo Pulmonary Squamous Cell Carcinoma Labeling in Small Animal Models

After determining optimized dosing and timing parameters, female athymic nude mice bearing pulmonary squamous cell carcinoma flank xenografts (n = 3 per cell line) were intravenously administered OTL78 at a dose of 2 mg/kg. Four hours after OTL78 injection, mice were euthanized and imaged with the Iridium Imaging System (Vision Sense, New York, NY). Tumors were removed and imaged with the Odyssey Imaging System (LI-COR Biosciences, Lincoln, NE). Tissue sections were further analyzed by hematoxylin and eosin staining, immunohistochemistry staining for PSMA, as well as fluorescence microscopy (Leica Microsystems, Wetzlar, Germany).

Results

Expression of PSMA in a Cohort of Patients with Resectable Pulmonary Squamous Cell Carcinoma

To first determine the clinical relevance of a PSMA-targeted tracer to guide surgical removal of pulmonary squamous cell carcinoma, we analyzed histologic specimens from 50 consecutive pulmonary squamous cell carcinoma resections (Table 1). Tumor cells and neovasculature endothelial cells (NECs) were examined. Of the examined specimens, 39 (78%) demonstrated PSMA expression within tumor cells (Figure 1A for representative examples). Twenty-one (42%) patients displayed PSMA overexpression with tumor cell staining of 2+ or 3+ intensity. On analysis of PSMA expression within NECs, 42 (84%) of tumors had PSMA-positive NECs (Figure 1B for representative example). Forty-seven (94%) of specimens displayed PSMA expression within either tumor cells or NECs, and these percentages remained high with increasing tumor stage (Figure 1C). On multivariate analysis, PSMA expression level was noted to be independent of several patient and histopathologic variables including patient age, patient gender, history of smoking, tumor stage, and self-reported race (Table 1).

Human Pulmonary Squamous Cell Carcinoma Cells are Fluorescently Labeled by OTL78 in a Time- and Concentration-Dependent Manner

Next, we sought to determine whether OTL78 (Figure 2A for molecular structure and absorption/emission spectra) would bind human pulmonary squamous cell carcinoma models *in vitro*. By flow cytometry, high levels of fluorescence were observed in the positive control 22rv1 (Figure 2B, mean MFI 3484), with no fluorescence in the negative control KB (mean MFI 239). Mild to moderate fluorescence was observed in both pulmonary squamous cell carcinoma cell lines (H1264 mean MFI=437, H513 mean MFI=506).

To assess the concentration-dependence of cell labeling, we incubated live H513 and H1264 cells with increasing concentrations of OTL78 and imaged them with fluorescence microscopy at 2 hours (Figure 2C). There was a clear dose-dependent relationship between concentration of OTL78 and fluorescence at the cellular level. Cellular fluorescence intensity began to plateau at the 50 nM concentration (mean MFI 43.2 A.U.).

To assess the localization and internalization of OTL78, we imaged live H1264 and H513 cells at various time points using fluorescence microscopy (Figure 2D). We found that OTL78 labeled cells with increasing total fluorescent signal over time. When viewed under 100x magnification (inset images), the probe was seen to move from the cell surface to the cytoplasm of the cell over time, presumably by PSMA-mediated endocytosis.

Optimal Dosing, Timing, and Biodistribution of OTL78 in Murine Xenografts

To determine the ideal dosing and timing of OTL78 in mice, we administered mice bearing 22rv1 and KB xenografts (tumor size 250 ± 50 mm^3, n=3 per group) escalating doses of OTL78 and imaged them at various points over the course of one week. In all groups, we appreciated strong background fluorescence immediately following injection (Figure 3A). At the lowest dosing levels (1 mg/kg and 2 mg/kg), fluorescence was predominantly observed in the tumor and kidneys by 2 hours.

TBRs above 2.0 were observed at 4 hours after injection in both the 1 mg/kg and 2 mg/kg dosing levels, with higher TBRs being noted in mice receiving OTL78 at 2 mg/kg (Figure 3B), 2.79 versus 2.23, $p = 0.04$). Mice receiving higher doses required a longer washout period, with clear demarcation of tumor fluorescence with TBR>2.0 not appearing until 8 hours after injection. After an adequate washout period, peak TBRs within the 4 mg/kg dosing group was 3.36. These values were similar to those observed in the animals dosed at 2 mg/kg ($p = 0.09$). These data suggested that the most effective and efficient dosing protocol involved delivery of 2 mg/kg with imaging occurring at 4 hours.

After establishing dosing parameters, we sought to evaluate OTL78 biodistribution. Three mice bearing 22rv1 xenografts and three mice bearing KB xenografts were administered 2 mg/kg of OTL78. After 4 hours, mice were euthanized and the fluorescence of multiple organs was obtained (Figure 3C). The highest levels of fluorescence were observed in kidneys (231 A.U.; Std Dev: 17 A.U.) and 22rv1 tumors (223 A.U.; Std Dev: 26 A.U.), with low background observed in the stomach and small bowel (Figure 3D). All other organs had minimal fluorescence. Importantly, the lungs of mice receiving the tracer had no background fluorescence, suggesting the utility of the tracer to clearly label pulmonary tumors.

OTL78 Fluorescently Labels Pulmonary Tumors in a Xenograft Mouse Model

To determine if OTL78 could label human pulmonary squamous cell carcinoma tumor xenografts, female athymic nude mice bearing H513 and H1264 xenografts were administered 2 mg/kg OTL78 via tail vein injection. Mice bearing 22rv1 xenografts were used as a positive control, and those bearing KB xenografts were used as a negative control. Four hours after OTL78 injection, mice were sacrificed and imaged with the Iridium NIR imaging system (Figure 4A).

Xenografts derived from both human pulmonary squamous cell carcinoma cell lines displayed strong macroscopic fluorescent signal that could be clearly delineated from background tissue. On post hoc analysis of fluorescent images, mean SBR was greater than 2.0 for all lung cancer xenografts, indicating excellent tumor-specific labeling (Figure 4B). The regions-of-interest corresponding to flank tumors had significantly higher MFI than those corresponding to background tissue in the same mice (Figure 4C). Mean tumor MFI in

the mice bearing H1264 xenografts was 92.45 A.U. (Std Dev 5.83 A.U.) and mean MFI in the mice bearing H513 xenografts was 113.78 A.U. (Std Dev 4.21 A.U.).

OTL78 Fluorescence Signal Correlates with PSMA Density

During our experiments in various cell lines, we noted a significant variation in the fluorescence between cell lines. In our animal experiments above, 22rv1 tumors consistently expressed the highest fluorescence followed by the pulmonary squamous cell carcinoma cell lines (H513 and H1264), with lowest levels of fluorescence in the KB xenografts. Based on these results coupled with *in vitro* analysis of PSMA expression, we postulated that the difference in fluorescence is attributable to differing levels of PSMA expression in the various tumors.

We examined the excised flank tumors by macroscopic tumor fluorescence imaging, hematoxylin and eosin staining, PSMA immunohistochemistry, and fluorescence microscopy (Figure 5A). We then performed a PSMA density analysis of the sectioned tumors by analyzing PSMA staining at the center and at four locations 90 degrees apart at the periphery. The percentage of PSMA-positive cells (2+ or 3+ staining) per high-powered field (HPF) was calculated and averaged per flank tumor. 22rv1 flank xenografts displayed the highest PSMA density with mean density of 97.3% (Figure 5B, Std Dev 0.9%) as compared to 66.7% (Std Dev 14.2%) in the H513 xenografts and 44.7% (Std Dev 10.5%) in the H1264 xenografts. PSMA density in the KB xenograft cohort was 7.7% (Std Dev 4.7%). These analyses were then correlated with macroscopic tumor MFI (Figure 5C). We found a robust correlation between PSMA density and tumor MFI (R^2=0.8506) thus providing one potential explanation for the difference in fluorescence between tumors.

OTL78 Identifies Residual Disease After Resection of Pulmonary Squamous Cell Carcinoma Xenografts

After identifying that OTL78 could label pulmonary squamous cell flank xenografts, we sought to determine if IMI using OTL78 could detect residual tumor deposits after resection. H513 and H1264 flank tumors (n=10 mice/group) were again established in female athymic nude mice. Once established, animals were administered OTL78 four hours prior to surgery. Animals were randomized to tumor resection with intentional positive margins (n=10) or complete removal (n=10). Subsequently, two blinded surgeons examined the wound beds for residual disease. Surgeons were not told the number of animals that had positive margins. One surgeon was only able to use conventional methods of finger palpation and visual inspection under white light. The other surgeon used traditional methods supplemented with IMI using OTL78 (Figure 6A).

Conventional methods correctly identified 7 residual tumors but missed 3 positive margins. There were 5 mice falsely assigned residual tumors by conventional methods, with sensitivity of 70% and specificity of 50%. Inspection aided by intraoperative NIR imaging was able to detect 9 true positive wound beds with 1 false negative diagnosis (Figure 6B). NIR imaging was not associated with any false positive diagnoses. Sensitivity and specificity of traditional methods augmented with IMI were 90% and 100%, respectively. The mean TBR of residual tumor deposits was 2.13 ± 0.21 (IQR 1.73–2.54, Figure 6C for

representative case). In summary, IMI significantly improved the diagnostic performance of traditional methods of detecting positive margins after resection.

Data Availability

The data that support the findings of this study are available from the corresponding author upon request.

Discussion

In this study, we validated a target for IMI during resection of pulmonary squamous cell carcinoma in a surgical cohort at our institution. We found high levels of PSMA expression in 94% of pulmonary squamous cell carcinoma resection specimens, in either the neovasculature endothelial cells or the tumor cells themselves. Building upon this finding, we then tested a PSMA-targeted IMI tracer (OTL78) in preclinical models of pulmonary squamous cell carcinoma and found that the tracer could quickly and selectively discriminate cancer cells and tumors from background tissue in a murine xenograft model. Furthermore, IMI using this tracer identified residual disease after resection with much greater sensitivity and specificity than conventional methods alone. These findings suggest the feasibility of clinical translation of OTL78 for IMI-guided resection of pulmonary squamous cell carcinoma.

Pulmonary squamous cell carcinoma arises from the thin, flat squamous cells that line the tracheobronchial tree of the lung.[27] Transformed squamous cells are characterized by keratinization or intercellular bridges and often exhibit a high degree of mutation frequency.[28] Despite the high mutation frequency, there are fewer actionable mutations in receptor tyrosine kinases in pulmonary squamous cell carcinoma as compared to pulmonary adenocarcinoma.[29] Therefore, these patients tend not to have a poorer response to systemic treatment as compared to other forms of non-small cell lung cancer.[30] For these reasons, early and complete surgical resection of disease is critically important in the prognosis of pulmonary squamous cell carcinoma.[31] However, early locoregional recurrence rates are high after resection due to incomplete clearance of microscopic disease that may not be visible to surgeons.[2] Adjuncts to traditional surgical methods to identify residual disease are urgently needed.

Intraoperative molecular imaging (IMI) is a technology that has gained traction in recent years to aid surgeons in achieving more complete resections.[32] IMI relies on systemically administered tracers that localize to cancer cells and can be detected using wavelength specific cameras.[33-36] IMI is a particularly attractive strategy to aid resection of lung cancers because they are often below the surface of the lung, and can be challenging to detect by visual inspection or manual palpation alone.[37,38] Our group has demonstrated that IMI significantly improves surgeons' ability to detect and remove pulmonary adenocarcinomas, but efforts to detect pulmonary squamous cell carcinomas have been hampered by the lack of a targeted tracer for this common and deadly histologic subtype of lung cancer.[39,40]

We hypothesized that PSMA would be an effective target for an IMI probe for pulmonary squamous cell carcinoma. PSMA, also termed GCP2, is a type II transmembrane protein

with intracellular, transmembrane, and extracellular domains.[16] It has been shown to regulate tumor cell invasion and angiogenesis by modulating integrin signal transduction in endothelial cells.[11] Importantly, PSMA is not expressed by normal lung parenchyma, allowing for development of tracers targeted specifically to cancer cells. Two recent studies of PSMA expression in non-small cell lung cancer (NSCLC) showed that pulmonary squamous cell carcinomas have the highest percentage of PSMA overexpression within all NSCLC subtypes.[10,11] Our findings that 94% of patients with surgically resectable pulmonary squamous cell carcinoma express PSMA in either tumor cells or NECs further validate PSMA as a target for IMI.

A number of PSMA-targeted IMI probes have been developed over the past decade and have shown significant promise in preclinical models of fluorescence-guided prostate cancer resection. [17,20,22-24] In 2005, Humblet and colleagues first described a small molecule based, PSMA-targeted IMI tracer for resection of prostate cancer in murine models.[41] Subsequently, other small molecule-based tracers[22,24] and an antibody-based probe[20] for PSMA have been studied. The use of OTL78 for detecting PSMA-positive prostate cancer cells was first described by Kularatne and colleagues.[17] Most recently, Zhang *et al* have developed a PSMA-targeted molecular rotor that becomes fluorescent upon PSMA binding.[25] All of these tracers have been developed and tested in models of prostate cancer surgery. Although applications of PSMA-targeted IMI tracers to other malignancies have been proposed[19], this is the first study to test the utility of a PSMA-targeted imaging agent for fluorescence guided resection of a non-prostatic malignancy.

The specific tracer evaluated in this study, OTL78, has a number of inherent advantages related to its molecular and optical properties that may help facilitate its rapid clinical translation. The fluorophore S0456 has peak emission in the near-infrared (NIR) range, which allows greater depth of tissue penetration as compared to IMI tracers in the visible, or far-red range.[42] Additionally, there is minimal autofluorescence of normal tissues in the NIR spectrum, allowing for more precise delineation between tumor tissue and normal lung parenchyma. OTL78 is a small molecule ligand which clears rapidly from PSMA-negative tissues, allowing IMI within 2-4 hours after infusion of the tracer. This timeline compares favorably with that required for antibody-tracer conjugates, which require at least 72 hours to clear from non-malignant tissues and necessitate a prolonged hospital stay or multiple hospital visits, leading to higher cumulative cost.[43] As OTL78 and other PSMA-targeted IMI agents progress toward clinical translation, patients will need to be closely monitored for toxicity relating to uptake of PSMA ligands by salivary glands, which has been seen in many PSMA-targeted radiopharmaceuticals.[44]

In summary, we have demonstrated that OTL78 binds *in vitro* and xenograft pulmonary squamous cell carcinoma models in a PSMA-dependent manner and can identify residual disease after resection in a preclinical model. Due to its high affinity and specificity for PSMA-expressing tumors, rapid clearance from normal tissues, and excellent safety profile, OTL78 has potential to become the first targeted NIR agent to enter into the clinic for use in fluorescence-guided resection of pulmonary squamous cell carcinoma. Further studies are needed to confirm its safety and efficacy, but it holds clear clinical promise for improving surgical management of patients with pulmonary squamous cell carcinoma.

Acknowledgments

Dr. Kennedy was supported by the American Philosophical Society and the National Institutes of Health (grant F32 CA254210-01). Dr. Azari was supported by the Society for Thoracic Surgeons. Dr. Singhal was supported by the National Institutes of Health (grant R01 CA193556) and the State of Pennsylvania Health Research Formula Fund.

References

1. Siegel RL, Miller KD, Fuchs HE, Jemal A. Cancer statistics, 2021. CA: A Cancer Journal for Clinicians. 2021;71(1):7–33. [PubMed: 33433946]
2. Aliperti LA, Predina JD, Vachani A, Singhal S. Local and systemic recurrence is the achilles heel of cancer surgery. Ann Surg Oncol. 2011;18(3):603–607. [PubMed: 21161729]
3. Predina JD, Keating J, Patel N, Nims S, Singhal S. Clinical implications of positive margins following non-small cell lung cancer surgery. J Surg Oncol. 2016;113(3):264–269. [PubMed: 26719121]
4. Lauwerends LJ, van Driel Pieter B. A. A, Baatenburg de Jong Robert J., et al. Real-time fluorescence imaging in intraoperative decision making for cancer surgery. Lancet Oncol. 2021.
5. Low PS, Henne WA, Doorneweerd DD. Discovery and development of folic-acid-based receptor targeting for imaging and therapy of cancer and inflammatory diseases. Acc Chem Res. 2008;41(1):120–129. [PubMed: 17655275]
6. Parker N, Turk MJ, Westrick E, Lewis JD, Low PS, Leamon CP. Folate receptor expression in carcinomas and normal tissues determined by a quantitative radioligand binding assay. Anal Biochem. 2005;338(2):284–293. [PubMed: 15745749]
7. Predina JD, Newton AD, Keating J, et al. A phase I clinical trial of targeted intraoperative molecular imaging for Pulmonary Adenocarcinomas. Ann Thorac Surg. 2018;105(3):901–908. [PubMed: 29397932]
8. Gangadharan S, Sarkaria I, Rice D, et al. Multi-institutional phase 2 clinical trial of intraoperative molecular imaging of lung cancer. Ann Thorac Surg. 2020.
9. Lu T, Yang X, Huang Y, et al. Trends in the incidence, treatment, and survival of patients with lung cancer in the last four decades. Cancer management and research. 2019;11:943–953. [PubMed: 30718965]
10. Wang H, Wang S, Song W, et al. Expression of prostate-specific membrane antigen in lung cancer cells and tumor neovasculature endothelial cells and its clinical significance. PLoS One. 2015;10(5):e0125924. [PubMed: 25978404]
11. Schmidt LH, Heitkötter B, Schulze AB, et al. Prostate specific membrane antigen (PSMA) expression in non-small cell lung cancer. PLoS One. 2017;12(10):e0186280. [PubMed: 29077706]
12. Bařinka C, Rojas C, Slusher B, Pomper M. Glutamate carboxypeptidase II in diagnosis and treatment of neurologic disorders and prostate cancer. Curr Med Chem. 2012;19(6):856–870. [PubMed: 22214450]
13. Anilkumar G, Rajasekaran SA, Wang S, Hankinson O, Bander NH, Rajasekaran AK. Prostate-specific membrane antigen association with filamin A modulates its internalization and NAALADase activity. Cancer Res. 2003;63(10):2645–2648. [PubMed: 12750292]
14. Rajasekaran SA, Anilkumar G, Oshima E, et al. A novel cytoplasmic tail MXXXL motif mediates the internalization of prostate-specific membrane antigen. Mol Biol Cell. 2003;14(12):4835–4845. [PubMed: 14528023]
15. Liu H, Rajasekaran AK, Moy P, et al. Constitutive and antibody-induced internalization of prostate-specific membrane antigen. Cancer Res. 1998;58(18):4055–4060. [PubMed: 9751609]
16. Kularatne SA, Wang K, Santhapuram HR, Low PS. Prostate-specific membrane antigen targeted imaging and therapy of prostate cancer using a PSMA inhibitor as a homing ligand. Mol Pharm. 2009;6(3):780–789. [PubMed: 19361233]
17. Kularatne SA, Thomas M, Myers CH, et al. Evaluation of novel prostate-specific membrane antigen-targeted near-infrared imaging agent for fluorescence-guided surgery of prostate cancer. Clin Cancer Res. 2019;25(1):177–187. [PubMed: 30201762]

18. Chang SS, Reuter VE, Heston WD, Bander NH, Grauer LS, Gaudin PB. Five different anti-prostate-specific membrane antigen (PSMA) antibodies confirm PSMA expression in tumor-associated neovasculature. Cancer Res. 1999;59(13):3192–3198. [PubMed: 10397265]
19. Derks YHW, Löwik Dennis W. P. M., Sedelaar JPM, et al. PSMA-targeting agents for radio- and fluorescence-guided prostate cancer surgery. Theranostics. 2019;9(23):6824–6839. [PubMed: 31660071]
20. Lütje S, Rijpkema M, Franssen GM, et al. Dual-modality image-guided surgery of prostate cancer with a radiolabeled fluorescent anti-PSMA monoclonal antibody. J Nucl Med. 2014;55(6):995–1001. [PubMed: 24700882]
21. Humblet V, Lapidus R, Williams LR, et al. High-affinity near-infrared fluorescent small-molecule contrast agents for in vivo imaging of prostate-specific membrane antigen. Mol Imaging. 2005;4(4):7290.2005.05163.
22. Derks YHW, Rijpkema M, Amatdjais-Groenen HIV, et al. Photosensitizer-based multimodal PSMA-targeting ligands for intraoperative detection of prostate cancer. Theranostics. 2021;11(4):1527–1541. [PubMed: 33408764]
23. Maurer T, Graefen M, van der Poel H, et al. Prostate-specific membrane antigen-guided surgery. J Nucl Med. 2020;61(1):6–12. [PubMed: 31732677]
24. Cordonnier A, Boyer D, Besse S, et al. Synthesis and in vitro preliminary evaluation of prostate-specific membrane antigen targeted upconversion nanoparticles as a first step towards radio/fluorescence-guided surgery of prostate cancer. J Mater Chem B. 2021;9(36):7423–7434. [PubMed: 34373887]
25. Zhang J, Rakhimbekova A, Duan X, et al. A prostate-specific membrane antigen activated molecular rotor for real-time fluorescence imaging. Nature communications. 2021;12(1):1–11.
26. Predina JD, Newton AD, Connolly C, et al. Identification of a folate receptor-targeted near-infrared molecular contrast agent to localize pulmonary adenocarcinomas. Mol Ther. 2018;26(2):390–403. [PubMed: 29241970]
27. Heist RS, Sequist LV, Engelman JA. Genetic changes in squamous cell lung cancer: A review. Journal of thoracic oncology. 2012;7(5):924–933. [PubMed: 22722794]
28. Travis WD, Brambilla E, Nicholson AG, et al. The 2015 world health organization classification of lung tumors: Impact of genetic, clinical and radiologic advances since the 2004 classification. J Thorac Oncol. 2015;10(9):1243–1260. [PubMed: 26291008]
29. Herbst RS, Morgensztern D, Boshoff C. The biology and management of non-small cell lung cancer. Nature. 2018;553(7689):446–454. [PubMed: 29364287]
30. Arbour KC, Riely GJ. Systemic therapy for locally advanced and metastatic Non–Small cell lung cancer: A review. JAMA. 2019;322(8):764–774. [PubMed: 31454018]
31. Yang CJ, Wang H, Kumar A, et al. Impact of timing of lobectomy on survival for clinical stage IA lung squamous cell carcinoma. Chest. 2017;152(6):1239–1250. [PubMed: 28800867]
32. Tringale KR, Pang J, Nguyen QT. Image-guided surgery in cancer: A strategy to reduce incidence of positive surgical margins. Wiley Interdiscip Rev Syst Biol Med. 2018;10(3):e1412. [PubMed: 29474004]
33. Kennedy GT, Azari FS, Callans D, Singhal S. Stellate ganglion localization using near-infrared intraoperative imaging during cardiac sympathetic denervation. Heart Rhythm. 2021.
34. Kennedy GT, Azari FS, Newton AD, et al. Use of near-infrared molecular imaging for localizing visually occult parathyroid glands in ectopic locations. JAMA Otolaryngol Head Neck Surg. 2021;147(7):669–671.. [PubMed: 33956088]
35. Kennedy GT, Newton A, Predina J, Singhal S. Intraoperative near-infrared imaging of mesothelioma. Transl Lung Cancer Res. 2017;6(3):279–284. [PubMed: 28713673]
36. Predina JD, Newton A, Kennedy G, Lee MK, Singhal S. Near-infrared intraoperative imaging can successfully identify malignant pleural mesothelioma after neoadjuvant chemotherapy. Mol Imaging. 2017;16:1536012117723785. [PubMed: 28856921]
37. Azari F, Kennedy G, Singhal S. Intraoperative detection and assessment of lung nodules. Surg Oncol Clin N Am. 2020;29(4):525–541. [PubMed: 32883456]
38. Kennedy GT, Azari FS, Bernstein E, et al. Targeted intraoperative molecular imaging for localizing nonpalpable tumors and quantifying resection margin distances. JAMA Surg. 2021.

39. Newton AD, Kennedy GT, Predina JD, Low PS, Singhal S. Intraoperative molecular imaging to identify lung adenocarcinomas. J Thorac Dis. 2016;8(Suppl 9):S697–S704. [PubMed: 28066672]

40. Kennedy GT, Okusanya OT, Keating JJ, et al. The optical biopsy: A novel technique for rapid intraoperative diagnosis of primary pulmonary adenocarcinomas. Ann Surg. 2015;262(4):602–609. [PubMed: 26366539]

41. Humblet V, Lapidus R, Williams LR, et al. High-affinity near-infrared fluorescent small-molecule contrast agents for in vivo imaging of prostate-specific membrane antigen. Mol Imaging. 2005;4(4):448–462. [PubMed: 16285907]

42. Hernot S, van Manen L, Debie P, Mieog JSD, Vahrmeijer AL. Latest developments in molecular tracers for fluorescence image-guided cancer surgery. The lancet oncology. 2019;20(7):e354–e367. [PubMed: 31267970]

43. Azari F, Kennedy G, Bernstein E, et al. Intraoperative molecular imaging clinical trials: A review of 2020 conference proceedings. J Biomed Opt. 2021;26(5).

44. Kalidindi TM, Lee S, Jou K, et al. A simple strategy to reduce the salivary gland and kidney uptake of PSMA-targeting small molecule radiopharmaceuticals. Eur J Nucl Med Mol Imaging. 2021;48(8):2642–2651. [PubMed: 33495926]

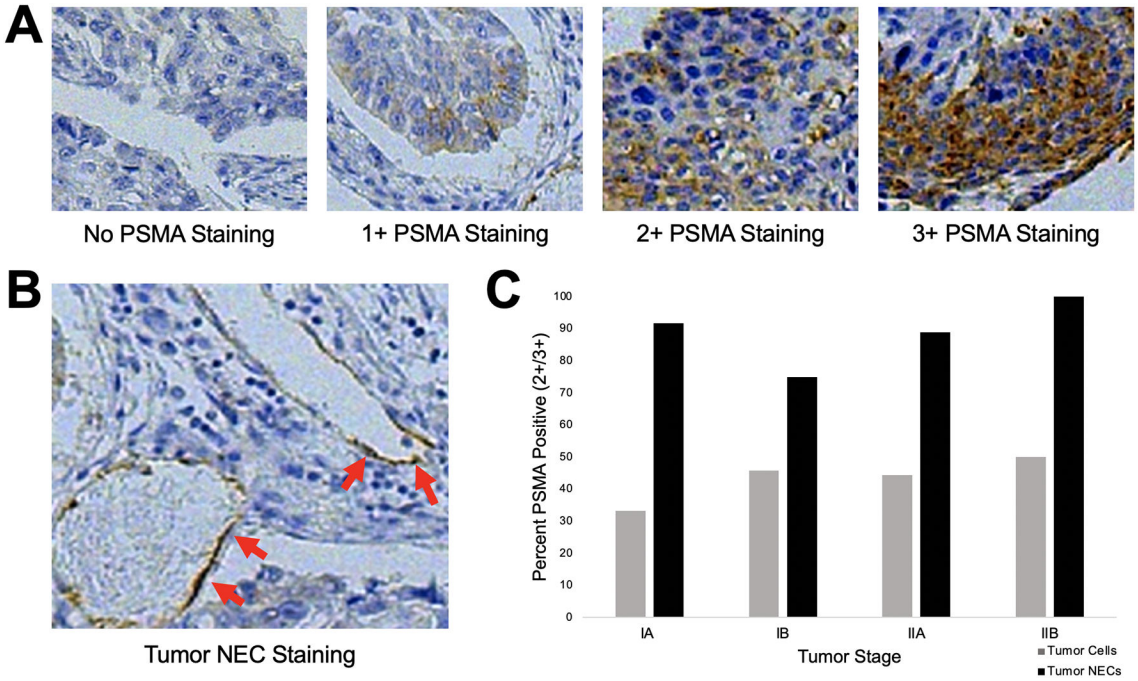

Figure 1.

Immunohistochemical analysis of PSMA expression in a cohort of patients with surgically resectable pulmonary squamous cell carcinoma. **A.** Representative staining intensities of pulmonary squamous cell carcinoma specimens scored as 0, no staining; 1+, weak staining; 2+, moderate staining; and 3+, strong staining. **B.** Representative image of PSMA-positive tumor neovascular endothelial (NEC) staining. **C.** Percent of specimens with PSMA expression in tumor cells or tumor NECs, stratified by final pathologic stage. PSMA was robustly expressed at all stages of disease and there were no significant differences by stage.

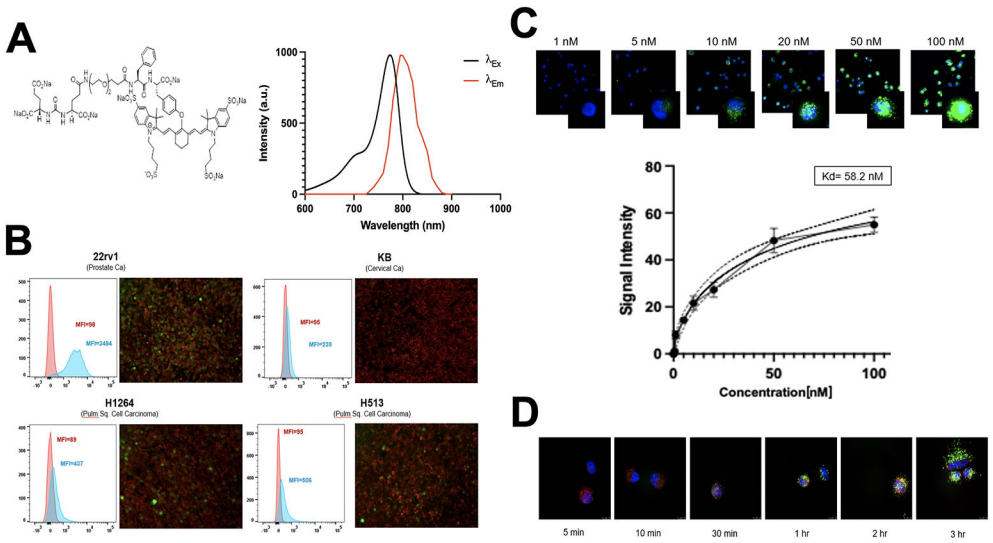

Figure 2.

Optical properties of OTL78 and *in vitro* labeling of human pulmonary squamous cell carcinoma cell lines. **A.** Chemical structure of OTL78 consisting of a high-affinity PSMA ligand coupled to the fluorophore S0456 (molecular weight: 1793.37 a.m.u.). Absorption and emission spectra at right show peak excitation at a wavelength of 774–776 nm and peak emission at 794–796 nm. **B.** *In vitro* OTL78 binding potential was evaluated for several human pulmonary squamous cell carcinoma lines. 22rv1 (a known high-PSMA-expressing prostate cancer cell line) was used as a positive control, while KB (a cervical carcinoma cell line with low PSMA expression) was used as a negative control. At left are representative flow cytometry tracings of cells after exposure to OTL78-spiked media (1 μM) for 4 hours. Mean fluorescence intensity (MFI) of OTL78-exposed cells corresponds to the blue histogram; unstained cells were used as a baseline (red histogram). Cells co-cultured with OTL78 were examined by fluorescence microscopy (green pseudocoloration) (right). Cells were counterstained with an anti-EPCAM antibody conjugated to a FITC fluorophore (red pseudocoloration). **C.** OTL78 labeling of human pulmonary squamous cell carcinoma cells (H513) in a concentration dependent manner. Cells were imaged 2 hours after OTL78 administration. OTL78 is shown in green overlaid upon DAPI staining. Inset images are at 100x. Kd by mean fluorescence intensity was calculated to be 58.2 nM. **D.** OTL78 labeling of human pulmonary squamous cell carcinoma cells (H513) in a time-dependent manner. OTL78 was administered at a concentration of 20 nM. OTL78 is shown in green overlaid upon DAPI staining. Inset images are at 100x.

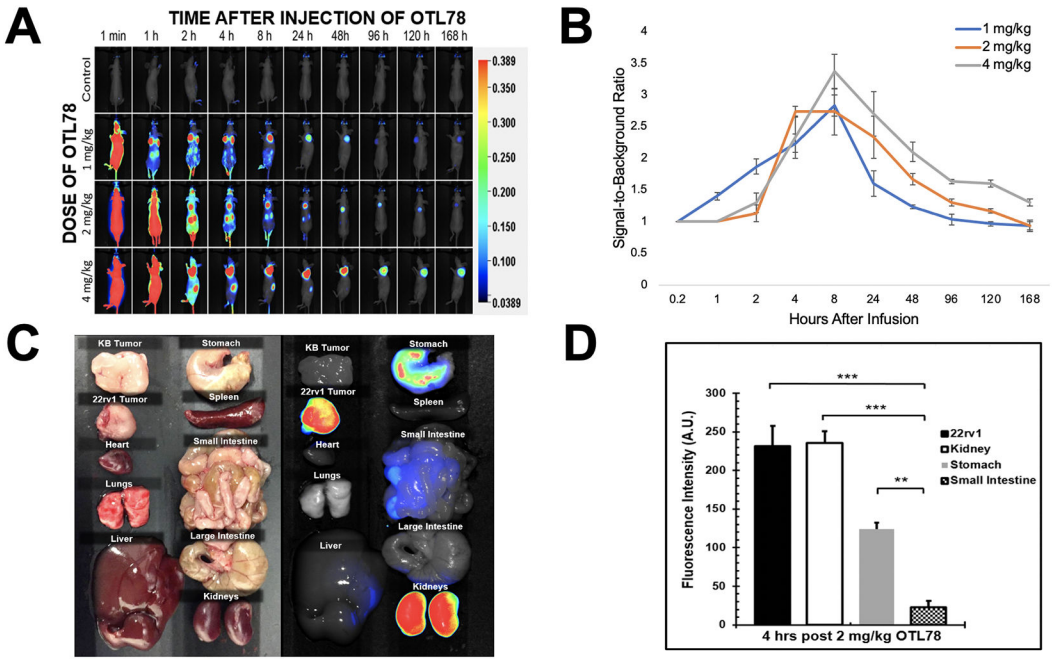

Figure 3.

Dosing, timing, and biodistribution of OTL78 in mice bearing flank xenografts. Mice bearing 22rv1 and KB flank xenografts were administered OTL78 at increasing dosing levels then imaged with the Pearl Trilogy *in vivo* Imaging System. **A**. Representative images of mice at various times after intravenous drug delivery. **B.** Signal-to background ratios (SBRs) were obtained for each dosing level and plotted over time from drug delivery. **C.** Four hours after delivery of OTL78 at 2 mg/kg, mice bearing 22rv1 and KB xenografts were euthanized to determine drug biodistribution. Fluorescence of organs and tumors were obtained using the Pearl Trilogy. **D.** Bar graph demonstrating fluorescence of flank tumors as compared to other organs.

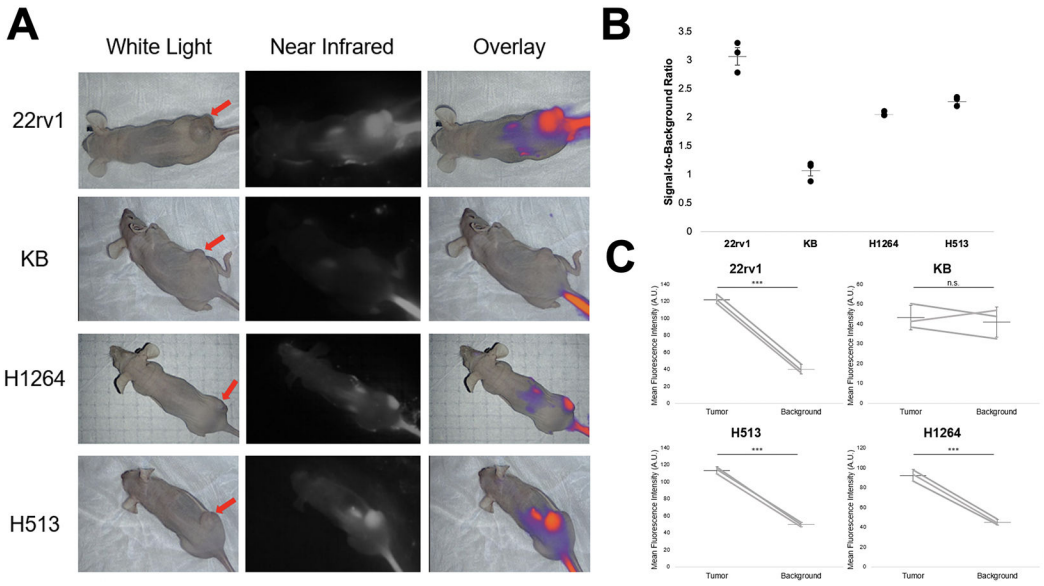

Figure 4.

OTL78 accumulates in pulmonary squamous cell carcinoma xenografts. Mice (n=3/group) bearing 22rv1, KB, H1264, and H513 flank xenografts were administered 2 mg/kg OTL78 and imaged with a NIR compatible imaging system four hours after injection. **A.** Representative images of mice from each group. The left column shows white light imaging with red arrow denoting the location of the flank xenograft. The center column shows near-infrared images, and the rightmost column shows NIR overlaid on white light image. **B.** SBRs from the flank xenografts. Each point represents a single tumor with means and error bars displayed for each group. **C.** Mean fluorescence intensity of tumor and background tissue. Lines represent paired tumor and background measurements from the same mouse. Mean bars with standard error are shown. ***: $p<0.0001$.n.s.: not significant.

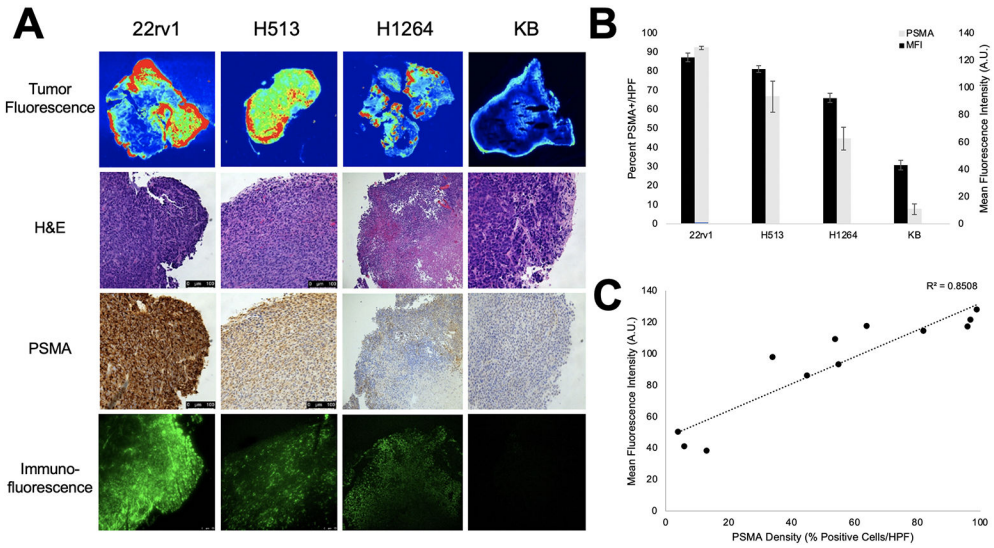

Figure 5.

Correlative *ex vivo* histopathology of flank xenografts and association of fluorescence with density of PSMA expression. All mice were administered 2 mg/kg OTL78 and mice were sacrificed 4 hours after OTL78 administration. **A.** Representative images from 22rv1, H513, H1264, and KB xenografts showing macroscopic tumor fluorescence, hematoxylin and eosin staining, immunohistochemical staining for PSMA, and immunofluorescence by fluorescence microscopy. **B.** Mean tumor MFI for each xenograft group plotted adjacently to PSMA density (% PSMA-positive cells/HPF) with error bars for the respective groups. **C.** Scatter plot of mean fluorescence intensity vs. PSMA density showing strong correlation between the two (R^2=0.8508). Each point represents a single tumor.

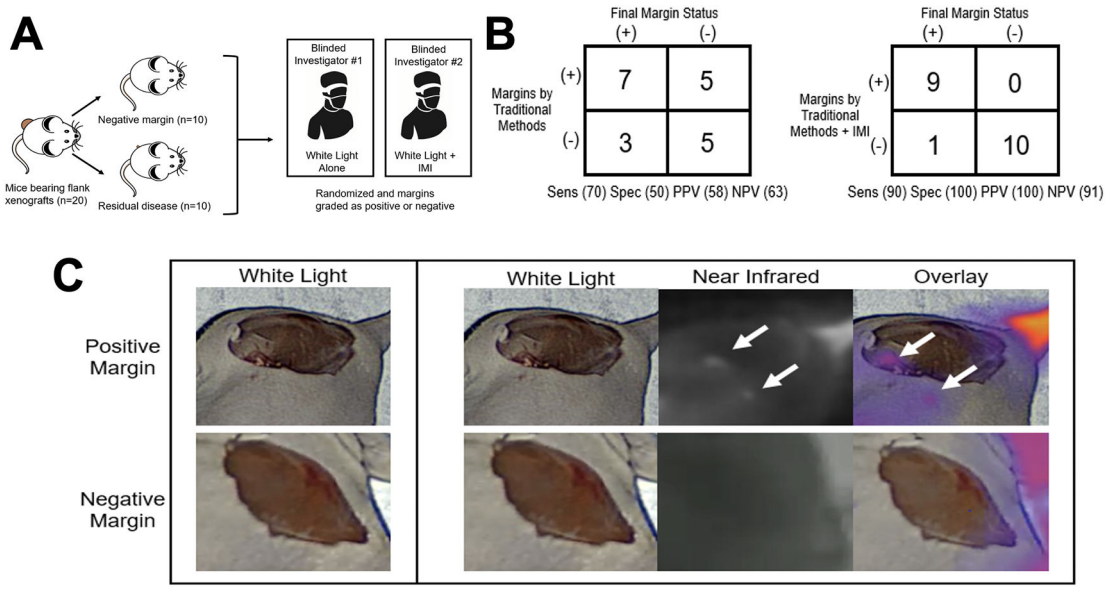

Figure 6.

IMI with OTL78 improves identification of residual disease after resection of pulmonary squamous cell carcinoma xenografts. **A.** Schematic of study design. Mice bearing H1264 and H513 flank xenografts (n=10/cell line) were randomized into resection with residual disease or complete (R0) resection. All mice were administered 2 mg/kg OTL78 and mice were sacrificed 4 hours after OTL78 administration. Two blinded surgeons were then asked to grade margins as positive or negative, without knowledge of the number of positive or negative margins. One investigator could use only traditional methods (visual inspection and finger palpation) and the other could use traditional methods aided by intraoperative imaging with OTL78. **B.** Summary of the accuracy of margins assessed by traditional methods alone compared to those assessed with the aid of OTL78 IMI. **C.** Representative images of positive and negative margins as seen by the surgeon using traditional methods (left column) and the one aided by IMI with OTL78 (rightmost three columns).

Table 1.

Multivariate model exploring PSMA expression with respect to patient/histopathologic characteristics in 50 patients who underwent resection of pulmonary squamous cell carcinoma. Values are presented as n (%) of patients unless otherwise indicated.

Variable	**PSMA Staining by Immunohistochemistry**							
	Tumor Cells					**Neovasculature Endothelial Cells**		
	0	**1+**	**2+**	**3+**		**PSMA−**	**PSMA+**	
Total (n, %)	11 (22.0)	18 (36.0)	17 (34.0)	4 (8.0)		8 (16.0)	42 (84.0)	
Gender								
Male (n=33)	8 (24.2)	11 (33.3)	11 (33.3)	3 (9.1)	p=0.923	5 (15.2)	28 (84.8)	p=0.821
Female (n=17)	3 (17.6)	7 (41.2)	6 (35.3)	1 (5.9)		3 (17.6)	14 (82.4)	
Age								
≤50 (n=6)	2 (33.3)	2 (33.3)	1 (16.7)	1 (16.7)	p=0.986	1 (16.7)	5 (83.3)	p=0.208
51-60 (n=16)	2 (12.5)	6 (37.5)	7 (43.8)	1 (6.3)		1 (6.3)	15 (93.7)	
61-70 (n=24)	5 (20.1)	10 (41.7)	8 (33.3)	1 (4.2)		5 (20.8)	19 (79.2)	
≥71 (n=4)	2 (50.0)	0 (0.0)	1 (25.0)	1 (25.0)		1 (25.0)	3 (75.0)	
Tumor Stage								
IA (n=12)	1 (8.3)	7 (58.3)	3 (25.0)	1 (8.3)	p=0.684	1 (8.3)	11 (91.7)	p=0.787
IB (n= 24)	6 (25.0)	7 (29.2)	8 (33.3)	3 (12.5)		6 (25.0)	18 (75.0)	
IIA (n=9)	3 (33.3)	2 (22.2)	4 (44.4)	0 (0.0)		1 (11.1)	8 (88.9)	
IIB (n=4)	1 (25.0)	1 (25.0)	2 (50.0)	0 (0.0)		0 (0.0)	4 (100.0)	
IIIA (n=1)	0 (0.0)	1 (100.0)	0 (0.0)	0 (0.0)		0 (0.0)	1 (100.0)	
Smoking History								
No (n=5)	2 (40.0)	2 (40.0)	1 (20.0)	0 (0.0)	p=0.083	2 (40.0)	3 (60.0)	p=0.127
Yes (n=45)	9 (20.0)	16 (35.6)	16 (35.6)	4 (8.9)		6 (13.3)	39 (86.7)	
Race								
White (n=35)	6 (17.1)	15 (42.9)	11 (31.4)	3 (8.6)	p=0.767	4 (11.4)	31 (88.6)	p=0.193
Black (n=11)	4 (36.4)	2 (18.2)	4 (36.4)	1 (9.1)		3 (27.3)	8 (72.7)	
Other (n=4)	1 (25.0)	1 (25.0)	2 (50.0)	0 (0.0)		1 (25.0)	3 (75.0)	